


Article

Magnetized Dissipative Soret Effect on Chemically Reactive Maxwell Fluid over a Stretching Sheet with Joule Heating

Suresha Suraiah Palaiah ¹, Hussain Basha ¹ , Gudala Janardhana Reddy ^{1,*} and Mikhail A. Sheremet ^{2,3,*}

¹ Department of Mathematics, Central University of Karnataka, Kalaburagi 585367, India; sureshasp94@gmail.com (S.S.P.); hussainbmaths@gmail.com (H.B.)

² Laboratory on Convective Heat and Mass Transfer, Tomsk State University, 634050 Tomsk, Russia

³ Butakov Research Center, National Research Tomsk Polytechnic University, 634050 Tomsk, Russia

* Correspondence: janardhanreddy.nitw@gmail.com (G.J.R.); sheremet@math.tsu.ru (M.A.S.)

Abstract: The present research paper deals with the study of heat and mass transfer characteristics of steady viscous incompressible two-dimensional Maxwell fluid flow past a stretching sheet under the influence of magnetic field and the Soret effect. A well-known non-Newtonian Maxwell fluid flow model is used to differentiate it from the Newtonian fluids. The present physical problem gives the set of highly nonlinear-coupled partial differential equations that are not amenable to any of the direct techniques. The resultant nonlinear system of partial differential equations is reduced to a set of nonlinear ordinary differential equations by using suitable similarity transformations. Due to the inadequacy of analytical techniques, a `bvp4c` MATLAB function is used to solve the developed nonlinear system of equations. The simulated results are shown for various values of physical parameters in the flow regime. Additionally, the numerical values of skin-friction coefficient, heat, and mass transfer rates are calculated and tabularized. From the present investigation, it is observed that the normal and axial velocity profiles decreased for the enhancing values of the magnetic parameter. Increasing the Prandtl and Schmidt numbers reduces the temperature and concentration profiles in the flow region, respectively. Increasing the Maxwell fluid parameter decreases the velocity profile and magnifies the temperature field. Additionally, increasing the Soret number increases the concentration profile in the flow regime. Comparison of current similarity solutions with available results indicates the accuracy and guarantee of the present numerical results and the used method.

Keywords: Maxwell fluid; Soret effect; magnetic number; Joule heating; Schmidt number



Citation: Suraiah Palaiah, S.; Basha, H.; Reddy, G.J.; Sheremet, M.A. Magnetized Dissipative Soret Effect on Chemically Reactive Maxwell Fluid over a Stretching Sheet with Joule Heating. *Coatings* **2021**, *11*, 528. <https://doi.org/10.3390/coatings11050528>

Received: 27 March 2021

Accepted: 23 April 2021

Published: 29 April 2021

Publisher's Note: MDPI stays neutral with regard to jurisdictional claims in published maps and institutional affiliations.



Copyright: © 2021 by the authors. Licensee MDPI, Basel, Switzerland. This article is an open access article distributed under the terms and conditions of the Creative Commons Attribution (CC BY) license (<https://creativecommons.org/licenses/by/4.0/>).

1. Introduction

Due to the exhaustive literature review, the analysis of boundary layer flow problems concerning real fluids past stretching sheets/surfaces received considerable attention in various fields of science and engineering including polymer sheet extrusion, metallurgy, drawing plastics, and chemical engineering. In the manufacturing of these physical materials, the melting issues from the slit and then stretches to attain the desired shape. In such physical problems, the magnetohydrodynamic (MHD) flows are significant and have greater technical applications in metallurgical and petroleum production industries. However, the characteristics of the end product significantly depend on the cooling rate, and these desired characteristics of the end product are controlled by utilizing electrically conducting fluids and the application of Lorentz forces. Further, in the purification of molten metals from nonmetallic additives, the applications of Lorentz forces play a key role. In addition to the above-mentioned applications and advantages, the investigation of thermal and mass transfer produced by stretching sheets/surfaces are of great significance in various industrial processes including hot rolling extrusion, crystal growing, glass blowing, rubber and plastic sheets, and spinning of fibers. However, among the available coolants, water is the most preferably utilized fluid. The analysis of flow and heat transfer in the above cases is very important because the accuracy of the end material

depends on wall shear stress and heat transfer rate. The detailed applications can be found in the literature [1].

For the first time, Sakiadis [2,3] investigated the different features of the stretching surface problems, particularly, the fluid flow over a horizontal semi-infinite moving surface in the free stream fluid. Phan-Thien [4] investigated the axisymmetric and plane stagnation point flow in a Maxwell fluid by using a shooting scheme. Zheng et al. [5] and Sadeghy et al. [6] analyzed the Sakiadis flow of hydrodynamic Maxwell fluid over a steadily moving rigid plate by using the boundary element method. Hayat et al. [7] discussed the flow of Maxwell fluid about a porous stretching surface by utilizing a homotopy analysis scheme. Further, the thermal transfer of Maxwell fluid in various stretching flow configurations was discussed by Hayat and Sajid [8], Abbas et al. [9,10], and Hayat et al. [11]. Ishak et al. [12] investigated the mixed convection flow about a vertical plate in a porous medium and analyzed the dual solutions close to the stagnation point. Sahoo [13] discussed the impact of MHD on thermal and flow behavior of conducting second-order fluid along an axisymmetric stretching surface with partial slip.

Ijaz and Ayub [14] discussed the influence of Cattaneo–Christov heat flux on the mixed convection flow of Jeffrey fluid over an elongating cylinder. It is recorded from their investigation that the increasing Deborah number raises the velocity field. Sandeep and Sulochana [15] analyzed the influence of nanofluids on temperature and velocity distributions over an elongating surface under the action of thermal source and sink. Their study reveals that amplifying radiation number magnifies the thermal field in the flow regime. The impact of thermal generation/absorption on magnetized Jeffrey nanofluid over an elongating cylinder was discussed by Ramzan et al. [16]. Their analysis shows that enhancing the stratification parameter diminished the thermal field. Khan et al. [17] demonstrated the influence of Soret and Dufour effects on Jeffrey fluid over an elongating cylinder under the action of Newtonian heat and mass transfer process. Hayat et al. [18] semi-analytically discussed the impact of mixed convection on Jeffrey liquid over an elongating cylinder with stratification conditions. Zeeshan and Majeed [19] discussed the influence of suction and injection on thermal transfer in Jeffrey fluid over an elongating sheet under the action of a magnetic dipole. The influence of Cattaneo–Christov heat flux on three-dimensional Jeffrey fluid flow over an elongating sheet was demonstrated by Hayat et al. [20]. Their investigation shows that the rising thermal relaxation time decays the thermal field. Abbasi et al. [21] studied the impact of thermal radiation on magnetized Jeffrey nanofluids over an elongating sheet under Brownian motion and thermophoresis. Hayat et al. [22] analyzed the impact of thermal radiation on an isothermally heated elongating cylinder under the action of viscous dissipation impact. Influence of thermal source/sink on magnetized Jeffrey fluid over elongating cylinder with Newtonian heating was discussed by Farooq et al. [23]. Hayat et al. [24] studied the time-independent axisymmetric flow of Jeffrey fluid under the action of thermophoresis and Brownian motion about an elongating cylinder.

The thermal flow of various viscoelastic fluids gained better consideration in industrial applications such as motor oils, polymer air processing, and spinning of various metals. Considerable investigations are readily available in the literature on the modeling of these heat transfer problems. In this direction, Liu and Guo [25] introduced a new fractional derivative method to analyze the Fourier law of heat conduction for unsteady Maxwell fluid with thermal radiation effect. Li et al. [26] discussed the thermal flow behavior of Maxwell liquid with improved fractional Darcy and Fourier law. Zhang et al. [27] described the impact of Marangoni convection on heat transfer behavior of power-law fluids with linear heat flow. Zhang et al. [28] investigated the impact of radiation on the heat transfer behavior of nanofluids over a flat plate with porosity effects having variable wall heat flux and chemical reaction. Shen et al. [29] analyzed the radiation impact on heat transfer of magnetized viscoelastic fluid via fractional derivative scheme over an unsteady stretching surface. Rachid [30] discussed the impacts of endoscope and heat flow on the peristaltic transfer of Maxwell fluid in a vertical cylindrical tube. Waheed [31] analyzed the heat and mass transfer of unsteady Maxwell fluid about a stretching sheet with radiation effect.

The temperature difference in the various parts of the material bodies result in heat energy transfer, and this phenomenon occurs in various biomedical, industrial processes. Additionally, it has a rich set of applications in heat conduction in energy generation, nuclear reactors, electronic equipment, mass transfer process, etc. The Fourier law of heat conduction [32] is the basic foundation for the understanding of heat transfer in flow fluid problems. Further, for any initial noise felt instantaneously in the material medium, the Fourier law of heat conduction provides the parabolic energy expression. However, the Fourier law of heat conduction appears physically unrealistic. Considering these drawbacks of the Fourier law of heat conduction, Cattaneo [33] revised this law by considering the relaxation time. Further, Christov [34] modified this law by considering the Oldroyd upper-convected derivatives. Tibullo and Zampoli [35] described the unique solution for the incompressible fluid flow problems by considering the Cattaneo–Christov heat flux model. Han et al. [36] studied the heat and flow behavior of Maxwell fluid about an elongating surface by utilizing the Cattaneo–Christov heat flux model. Detailed information on heat transfer studies can be found in the literature [37–40].

Srinivasulu and Goud [41] discussed the effect of magnetic field on Williamson nanofluid flow over a stretching sheet under the action of convective boundary conditions. It is noticed from their investigation that the temperature field is enhanced with the rising Prandtl number. Khan and Sultan [42] investigated the magnetized Williamson liquid over a rotating disk under the action of Soret and Dufour effects. From their analysis, it is found that radial velocity enhances with rising radial slip parameter. Shafiq et al. [43] discussed the mixed convection stagnation point flow of Williamson fluid over a vertical elongating plate. It is recorded from the analysis that the boundary layer thickness is enhanced with increasing Grashof and Eckert numbers. Rasool et al. [44] described the flow of Williamson nanofluid over a nonlinear stretching surface under the influence of entropy generation and chemical reaction. Their analysis shows that the Bejan number is increased with the rising of the Weissenberg number. Hamid et al. [45] investigated the unsteady Williamson fluid flow over an elongating sheet with multiple slip conditions under the action of a chemical reaction. Hashim [46] discussed the influence of magnetic field on Williamson nanofluid flow over an expanding/contracting cylinder under the influence of convective boundary conditions with multiple solutions. It is found that the accelerating magnetic parameter magnifies the velocity field in the flow regime. Khan et al. [47] described the impact of entropy generation on Williamson nanofluid over an elongating sheet under the action of Joule heating and chemical reaction effects. Khan et al. [48] discussed the influence of variable thermal coefficient and activation energy on magnetized Williamson nanofluid flow over a rotating stretching surface under the impact of thermal radiation effect.

The mass flow is the motion of the concentration field from one location to another location, and this convective mass transport behavior is greatly used in different engineering systems, for instance, water evaporation, chemical contamination diffusion in rivers and oceans, and chemical separation in the distillation process. The mass flow process has a rich set of technical applications in the chemical engineering field. Usually, the chemical species transfer occurs between two different stages of the flow phenomena through the diffusion process. Concentration difference is the main driving force behind the mass flow; the zig-zag movement of species causes the net mass flow from a location of higher concentration to a location of lower concentration. Thermodynamics identifies the extent of separation for the separation processes; on the other hand, mass flow identifies the possible separation rate. However, the quantity of mass flow can be measured with the help of calculations and the use of mass transport coefficients. In this direction, the following is the available literature review in mass flow under various aspects. Kendoush [49] analyzed the stagnation point flow with thermal and mass transfer to liquid jets imposing usually on solid walls. Liu [50] investigated the hydromagnetic flow about an elongating sheet with thermal and concentration transfer. Cortell [51] studied the chemically reactive mass flow species for two different groups of viscoelastic fluids about a porous elongating surface. Andersson et al. [52] examined the transport of momentum and chemically reactive

species concentration about a linearly elongating sheet. Takhar et al. [53] investigated the magnetized heat and flow behavior of viscous fluid over an elongating surface with slip velocity. Further, Akyildiz et al. [54] studied the chemically reactive species diffusion about an elongating sheet under the influence of a porous medium. Layek et al. [55] described the impact of thermal absorption/generation and suction/blowing on boundary layer behavior of heat and mass transfer characteristics of stagnation-point flow about a heated porous stretching surface. Hayat et al. [56] discussed similar solutions of stretching flows with concentration transport effects. Further, Hayat and Awais [57] described the simultaneous influence of thermal and concentration transport on an unsteady fluid motion about a stretching surface.

Raza et al. [58] discussed the influence of viscous and Joule heating effects on multiple slip flow of Williamson nanofluid over a slandering stretching plate under the impact of temperature-dependent conductivity. Their investigation shows that increasing the Williamson fluid parameter increases the thermal field. Shawky et al. [59] discussed the influence of Soret and Dufour effects on Williamson nanofluid over an elongating sheet under the influence of a porous medium. It is recorded from their analysis that the Nusselt number diminished with the rising radiation absorption parameter. Loganathan and Rajan [60] analyzed the influence of Joule heating and convective heating on Williamson nanofluid over a stretching surface under the influence of Christov–Cattaneo heat flux. Salahuddin [61] studied the behavior of time-dependent Williamson fluid about a permeable stretching surface. Their investigation shows that the Williamson fluid is a decreasing function of fluid motion in the flow regime. Dada and Onwubuya [62] discussed the impact of magnetic field on flow and heat transfer behavior of Williamson fluid over a slendering elongating sheet. Their analysis shows that enhanced Lorentz forces diminished the flow velocity. Kumar et al. [63] analyzed the impact of nonlinear thermal radiation and Joule heating on Williamson nanofluid over a stretching sheet under the influence of entropy generation. Khan et al. [64] discussed the effect of magnetic field on non-Newtonian Williamson fluid over a stretchable rotating disk. Their analysis described that the increasing Williamson liquid parameter decays the radial velocity field in the flow regime.

Based on the current literature review, it is noticed that the problem considered in this study has a good number of applications in the various fields of engineering. According to the authors' knowledge, the steady-state boundary layer flow of Maxwell fluid over a stretching sheet with the above-mentioned physical effects has not yet been reported in the literature. Thus, the authors made an attempt to investigate the thermal and concentration transport characteristics of Maxwell fluid over a stretching sheet with magnetic effect by using the `bvp4c` MATLAB function. Further, the authors discussed the physical behavior of the skin-friction coefficient, heat, and mass transport rates. Additionally, figures and tables are shown to express the thermodynamic nature of various control parameters on local profiles.

The structure of this research article is classified into six sections. Section 1 illustrates the introduction and brief literature review. Section 2 describes the rheological behavior of Maxwell fluid. Section 3 illustrates the mathematical formulation. The numerical solution procedure is illustrated in Section 4. Simulated results are discussed in Section 5. Finally, conclusions of the considered problem are summarized in Section 6.

2. Cauchy Stress Tensor for Maxwell Fluid

The stress–strain relationship of viscous incompressible non-Newtonian Maxwell fluid is stated using the following Cauchy stress tensor (\mathbf{T}) [6]:

$$\mathbf{T} = -p\mathbf{I} + \mathbf{S} \quad (1)$$

In the above Equation (1), the identity vector is denoted by \mathbf{I} , p is the pressure, and the value of extra stress tensor \mathbf{S} is obtained as follows:

$$\mathbf{S} + \lambda \left(\frac{D\mathbf{S}}{Dt} \right) = \mu \cdot \mathbf{A}_1 \quad (2)$$

In the above Equation (2), viscosity is denoted with μ , relaxation time is λ , D/Dt is the covariant derivative, and Rivlin–Erickson tensor \mathbf{A}_1 is stated as follows:

$$\frac{D\mathbf{S}}{Dt} = \frac{d\mathbf{S}}{dt} - \mathbf{L}\mathbf{S} - \mathbf{S}\mathbf{L}^T \quad (3)$$

$$\mathbf{A}_1 = \text{grad}(\mathbf{V}) + [\text{grad}(\mathbf{V})]^T \quad (4)$$

In the above Equation (3), d/dt is substantial time derivation and in Equation (4), \mathbf{V} is the flow field, and the value of \mathbf{L} in Equation (3) is defined as follows:

$$\mathbf{L} = [\text{grad}(\mathbf{V})] \text{ and } \mathbf{L}^T = [\text{grad}(\mathbf{V})]^T \quad (5)$$

3. Mathematical Definition of the Problem

The present research article investigates the effect of magnetic field on flow and heat transfer characteristics of time-independent viscous incompressible Maxwell fluid with Joule heating and viscous dissipation effect numerically. In the present analysis, the Maxwell fluid flow is confined to the plane $y > 0$. The nonlinear flow and the heat transfer system are considerably simplified by subjecting them to the boundary-layer approximations. However, the Cartesian coordinate system is implemented to describe the considered physical problem in which the x -coordinate is measured along the flow direction, and the y -axis is chosen perpendicular to the x -axis. The geometry of the present physical problem is illustrated in Figure 1.

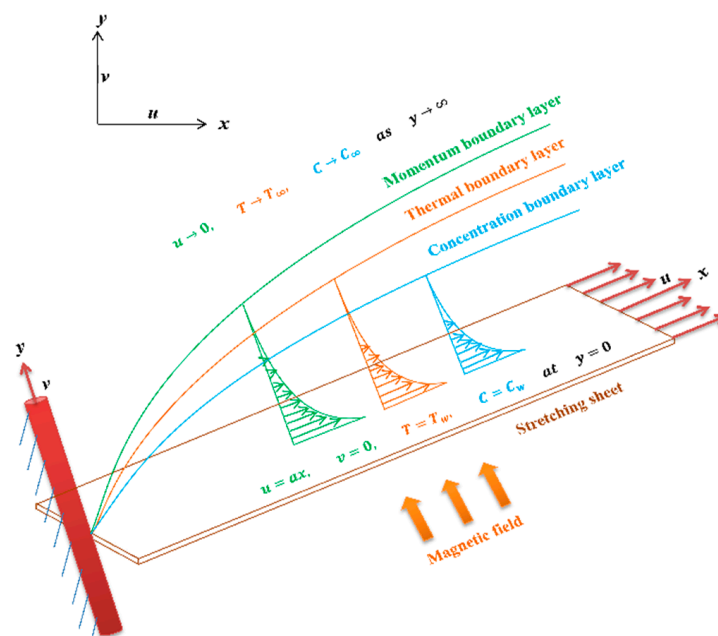


Figure 1. Analyzed geometry with boundary conditions and coordinates.

Further, a uniform magnetic field B_0 is applied normally to the x -axis. Additionally, due to the influence of equal and opposite forces, the surface is stretched over the flow direction with a fixed origin. However, due to the stretching of the sheet along the x -axis, the fluid flow occurred. Further, it is assumed that the surface of the stretching sheet is maintained at a wall temperature T_w and wall concentration C_w . Additionally, T_w and

C_w are supposed to be greater than free stream temperature T_∞ and concentration C_∞ . With the help of the above assumptions and boundary layer assumptions, the steady-state governing Maxwell fluid flow equations [6,65,66] are listed as follows:

$$\frac{\partial u}{\partial x} + \frac{\partial v}{\partial y} = 0 \quad (6)$$

$$u \frac{\partial u}{\partial x} + v \frac{\partial u}{\partial y} = \nu \frac{\partial^2 u}{\partial y^2} - \lambda \left(u^2 \frac{\partial^2 u}{\partial x^2} + v^2 \frac{\partial^2 u}{\partial y^2} + 2uv \frac{\partial^2 u}{\partial x \partial y} \right) - \frac{\sigma B_0^2}{\rho} u \quad (7)$$

$$u \frac{\partial T}{\partial x} + v \frac{\partial T}{\partial y} = \frac{k}{\rho C_p} \frac{\partial^2 T}{\partial y^2} + \frac{\mu}{\rho C_p} \left(\frac{\partial u}{\partial y} \right)^2 + \frac{\sigma B_0^2}{\rho C_p} u^2 \quad (8)$$

$$u \frac{\partial C}{\partial x} + v \frac{\partial C}{\partial y} = D_m \frac{\partial^2 C}{\partial y^2} - k_1(C - C_\infty) + \frac{D_m K_T}{T_m} \frac{\partial^2 T}{\partial y^2} \quad (9)$$

The partial differential Equations (6)–(9) are governed by the following boundary conditions:

$$\left. \begin{aligned} u &= u_w(x) = ax, v = 0, T = T_w, C = C_w \text{ at } y = 0 \\ u &\rightarrow 0, T \rightarrow T_\infty, C \rightarrow C_\infty \text{ as } y \rightarrow \infty \end{aligned} \right\} \quad (10)$$

In the above Equations (6)–(10), u , v are the velocities in x and y directions, T and C are the temperature and concentration, ρ is the density, D_m is the diffusion parameter, and a is the positive constant.

3.1. Implementation of Similarity Transformations

The system of complex coupled partial differential equations (PDEs) are reduced to the set of ordinary differential equations (ODEs) through suitable similarity transformations. Thus, the used similarity transformations [65] for the present problem are listed below.

$$\left. \begin{aligned} \eta &= y\sqrt{a/\nu} \\ \psi &= xf\sqrt{a\nu} \\ u &= axf'(\eta) \\ v &= (-\sqrt{a\nu})f(\eta) \\ \theta(\eta) &= \frac{T-T_\infty}{T_w-T_\infty} \\ \phi(\eta) &= \frac{C-C_\infty}{C_w-C_\infty} \end{aligned} \right\} \quad (11)$$

In the above Equation (11), η is the similarity variable, θ is the dimensionless temperature, ϕ is the dimensionless concentration, ψ is the stream function, and u , v are the velocity components along x and y directions, respectively.

3.2. Governing Equations in Terms of Similarity Variable Implementation

Thus, the transformations defined in terms of similarity variable η automatically obey the law of conservation of mass Equation (6). Further, the governing partial differential Equations (6)–(9) in terms of similarity variable (see Equation (11)) are summarized as follows:

$$f'''(\eta) + f(\eta)f''(\eta) - [f'(\eta)]^2 - Mf'(\eta) + \beta [2f(\eta)f'(\eta)f''(\eta) - f^2(\eta)f'''(\eta)] = 0 \quad (12)$$

$$\theta''(\eta) + \text{Pr}f(\eta)\theta'(\eta) + \text{PrEc}\{[f''(\eta)]^2 + M[f'(\eta)]^2\} = 0 \quad (13)$$

$$\phi''(\eta) + \text{Sc}f(\eta)\phi'(\eta) - \text{ScKr}\phi(\eta) + \text{SrSc}\theta''(\eta) = 0 \quad (14)$$

Additionally, the governing boundary conditions in terms of Equation (11) are stated as follows:

$$\left. \begin{aligned} f(0) = 0, f'(0) = 1, \theta(0) = 1, \phi(0) = 1 & \quad \text{at } \eta = 0 \\ f'(\infty) \rightarrow 0, \theta(\infty) \rightarrow 0, \phi(\infty) \rightarrow 0 & \quad \text{as } \eta \rightarrow \infty \end{aligned} \right\} \quad (15)$$

In Equations (12)–(15), the superscript symbol prime indicates the differentiation with respect to η . Further, dimensionless numbers involved in the above governing Equations (12)–(14) are summarized as follows:

$M = \sigma B_0^2 / (\rho a)$ is the magnetic parameter, $\beta = a\lambda$ is the Maxwell fluid parameter, $Pr = \nu / \alpha$ is the Prandtl number, $Ec = u_w^2 / \{C_p(T_w - T_\infty)\}$ is the Eckert number, $Sc = \nu / D_m$ is the Schmidt number, $Kr = k_1 / a$ is the chemical reaction parameter, and $Sr = \{D_m K_T / (\nu T_m)\} (T_w - T_\infty) / (C_w - C_\infty)$ is the Soret number.

3.3. Engineering Quantities of Interest

Knowing the steady-state flow behavior, temperature and concentration distributions profiles from the solution of the Equations (12)–(14) with essential boundary conditions given in Equation (15), it is worth studying the behavior of local skin-friction coefficient (Cf_x), the Nusselt number (Nu_x) and the Sherwood number (Sh_x) with respect to different physical parameters. For the present problem, the non-dimensional local skin-friction coefficient and Nusselt and Sherwood numbers are given as follows [6,65]:

$$Cf_x = \frac{\tau_w}{\rho u_w^2} \quad (16)$$

$$Nu_x = \frac{xq_w}{k(T_w - T_\infty)} \quad (17)$$

$$Sh_x = \frac{xq_m}{D_m(C_w - C_\infty)} \quad (18)$$

In the above Equations (16)–(18), the wall shear stress (τ_w), heat flux (q_w), and mass flux (q_m) are taken as follows:

$$\tau_w = \mu \left(\frac{\partial u}{\partial y} \right)_{y=0} \quad (19)$$

$$q_w = -k \left(\frac{\partial T}{\partial y} \right)_{y=0} \quad (20)$$

$$q_m = -D_m \left(\frac{\partial C}{\partial y} \right)_{y=0} \quad (21)$$

Finally, the non-dimensional equations of skin-friction coefficient and heat and mass transport rates in view of Equation (11) are obtained as follows:

$$Cf_x Re_x^{0.5} = f''(0) \quad (22)$$

$$Nu_x Re_x^{-0.5} = -\theta'(0) \quad (23)$$

$$Sh_x Re_x^{-0.5} = -\phi'(0) \quad (24)$$

Here, $Re_x = ax^2 / \nu$ is the local Reynolds number.

4. Computational Procedure

The considered physical problem is governed by the system of complex coupled PDEs and which are diminished to the system of ODEs by using suitable similarity transformations. Further, the reduced system of nonlinear ODEs (12)–(14) is simplified by utilizing

the bvp4c MATLAB function [67]. To this end, the system of ODEs (12)–(14) is reduced to first-order ODEs, which are summarized as follows:

$$\left. \begin{aligned} \frac{df_0}{d\eta} &= f_1 \\ \frac{df_1}{d\eta} &= f_2 \\ \frac{df_2}{d\eta} &= \frac{f_1^2 + Mf_1 - f_0f_2 - 2\beta f_0f_1f_2}{1 - \beta f_0^2} \end{aligned} \right\} \quad (25a)$$

$$\left. \begin{aligned} \frac{d\theta_0}{d\eta} &= \theta_1 \\ \frac{d\theta_1}{d\eta} &= -\text{PrEc}(Mf_1^2 + f_2^2) - \text{Pr}f_0\theta_1 \end{aligned} \right\} \quad (25b)$$

$$\left. \begin{aligned} \frac{d\phi_0}{d\eta} &= \phi_1 \\ \frac{d\phi_1}{d\eta} &= -\text{Sc}\left(f_0\phi_1 - \text{Kr}\phi_0 + \text{Sr}\frac{d\theta_1}{d\eta}\right) \end{aligned} \right\} \quad (25c)$$

In the above Equation (25a–c), we have considered $f(\eta) = f_0(\eta)$, $\theta(\eta) = \theta_0(\eta)$ and $\phi(\eta) = \phi_0(\eta)$. Additionally, the required initial and boundary conditions to solve Equation (25a–c) are listed as follows:

$$\left. \begin{aligned} f_0 &= 0, f_1 = 1 & \text{at } \eta = 0 \\ f_1 &\rightarrow 0 & \text{as } \eta \rightarrow \infty \end{aligned} \right\} \quad (26)$$

$$\left. \begin{aligned} \theta_0 &= 1 & \text{at } \eta = 0 \\ \theta_0 &\rightarrow 0 & \text{as } \eta \rightarrow \infty \end{aligned} \right\} \quad (27)$$

$$\left. \begin{aligned} \phi_0 &= 1 & \text{at } \eta = 0 \\ \phi_0 &\rightarrow 0 & \text{as } \eta \rightarrow \infty \end{aligned} \right\} \quad (28)$$

Thus, the set of first-order ODEs (25a–c) with conditions (26)–(28) is simplified by employing the bvp4c MATLAB function. The mathematical computations are conducted by choosing step size $\Delta\eta = 0.01$ and convergence criteria is 10^{-3} .

5. Results and Discussion

The heat and mass transport characteristics of steady Maxwell fluid flow over a stretching sheet has been studied under the influence of magnetic field through bvp4c MATLAB solver. The numerical data are generated for various values of available control parameters such as β (Maxwell fluid parameter), M (magnetic parameter), Pr (Prandtl number), Ec (Eckert number), Kr (chemically reaction parameter), Sr (Soret number), and Sc (Schmidt number) within the boundary layer region. These results are presented in terms of tables and graphs.

5.1. Validation of Present Solutions

The accuracy of solutions obtained based on bvp4c MATLAB solver is validated with solutions generated through classical Runge–Kutta method with shooting procedure in the limiting sense for different values of Maxwell fluid parameter, which are tabulated in Table 1. Table 1 guaranteed that the present solutions are matching remarkably with the results of Abel et al. [65] and Sadeghy et al. [66]. The excellent agreement is an encouragement for the authors to analyze the effects of various control variables on Maxwell fluid flow over a stretching sheet.

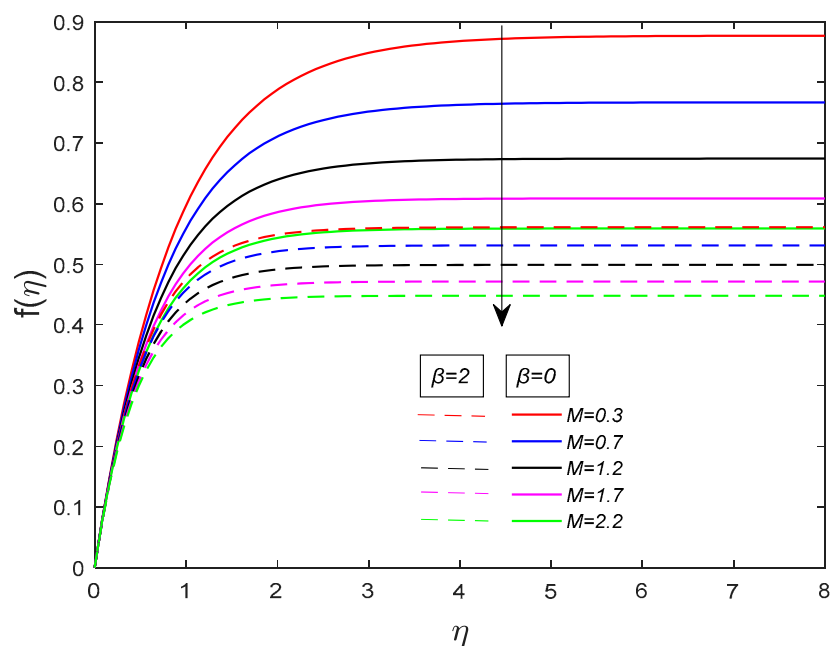
Table 1. Comparison of present solutions with Abel et al. [65] and Sadeghy et al. [66].

Parameter	Numerical Values of Skin-Friction Coefficient $f''(0)$				
	Sadeghy et al. [66]	Abel et al. [65]		Present solutions	
$\beta = 0$	$M = 0$ −1.0000	$M = 0$ −0.999962	$M = 0.2$ −1.095445	$M = 0$ −1.0000	$M = 0.2$ −1.095456

5.2. Influence of Governing Parameters

5.2.1. Impact of the Magnetic Number (M)

The effect of the magnetic number on flow profiles with ($\beta = 0$) and ($\beta = 2$) is depicted in Figures 2–5. The impact of magnetic parameter on $f(\eta)$ and $f'(\eta)$ profiles are shown in Figures 2 and 3. Figures 2 and 3 describe that the $f(\eta)$ and $f'(\eta)$ profiles diminished for the rising values of magnetic number. Enhancing magnetic number increases the Lorentz force in the flow region and hence the flow profiles are diminished. However, the velocity field is significant for $\beta = 0$, when compared to $\beta = 2$. Figures 4 and 5 describe the impact of the magnetic number on thermal and concentration distribution for $\beta = 0$ and $\beta = 2$. Enhancing the magnetic number magnifies the thermal distribution. Additionally, the thermal boundary layer thickens for higher values of the magnetic number. Furthermore, the increased temperature field is due to the enhanced Lorentz force, and it dissipates more heat energy into the flowing fluid, and thereby, the temperature field shows the increasing behavior. Further, Figure 5 shows that the magnifying magnetic number enhances the concentration profile. Additionally, the concentration boundary layer is observed to be thicker for higher values of the magnetic parameter.

**Figure 2.** Effect of magnetic parameter (M) on normal velocity profile with $Pr = Sc = 0.7$, $Ec = Kr = Sr = 0.1$.

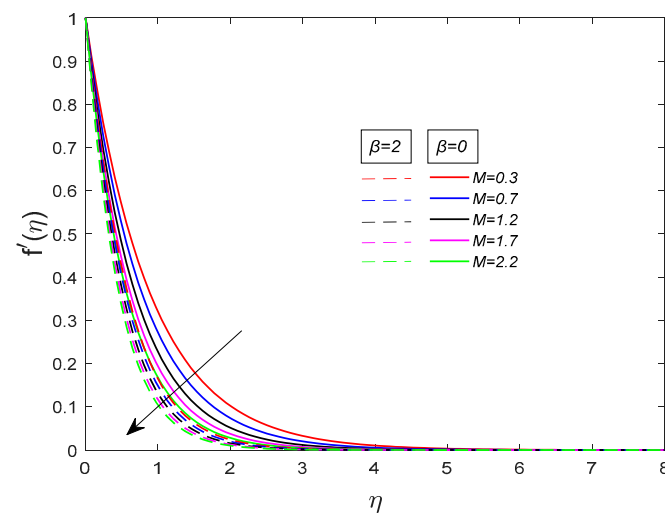


Figure 3. Effect of magnetic parameter (M) on axial velocity profile with $Pr = Sc = 0.7$, $Ec = Kr = Sr = 0.1$.

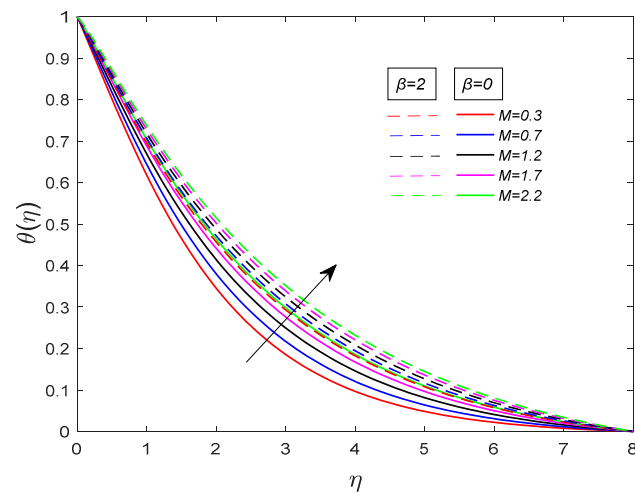


Figure 4. Effect of magnetic parameter (M) on temperature profile with $Pr = Sc = 0.7$, $Ec = Kr = Sr = 0.1$.

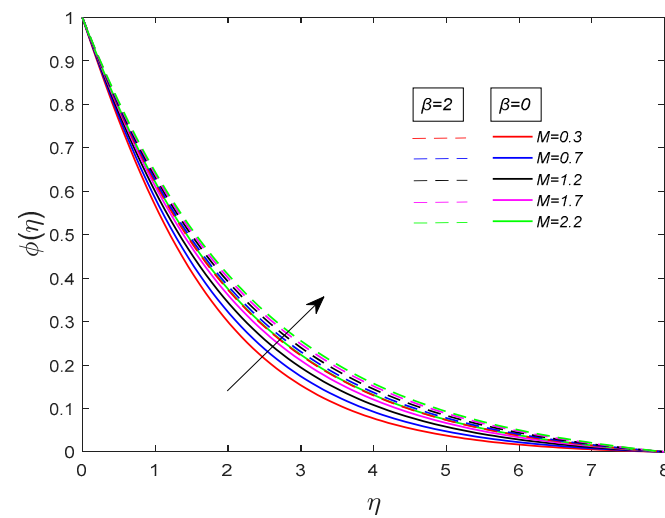


Figure 5. Effect of magnetic parameter (M) on concentration profile with $Pr = Sc = 0.7$, $Ec = Kr = Sr = 0.1$.

5.2.2. Impact of Maxwell Fluid Parameter (β)

The impact of the Maxwell fluid parameter on the flow field is demonstrated in Figures 6–9. Figures 6 and 7 illustrate that the $f(\eta)$ and $f'(\eta)$ profiles diminished for the rising values of β . Since increasing Maxwell fluid parameter offers increasing resistance to the flow, $f(\eta)$ and $f'(\eta)$ decreased in the flow regime. Additionally, the momentum boundary layer is diminished for the rising values of the Maxwell fluid parameter. Figure 8 describes the impact of the Maxwell fluid parameter on the temperature profile. Enhancing the Maxwell number magnifies the thermal profile. Further, the influence of β on concentration distribution is shown in Figure 9. It is recorded from Figure 9 that the magnifying β raises the concentration profile in the flow regime and the concentration boundary layer thickens for rising β .

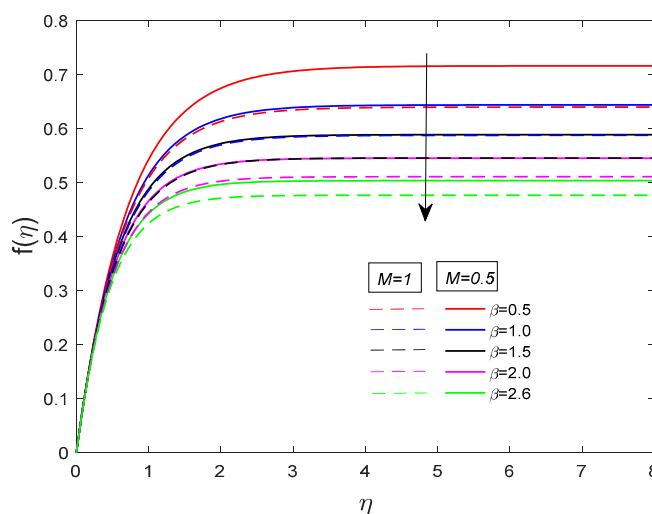


Figure 6. Effect of Maxwell fluid parameter (β) on normal velocity profile with $Pr = Sc = 0.7$, $Ec = Kr = Sr = 0.1$.

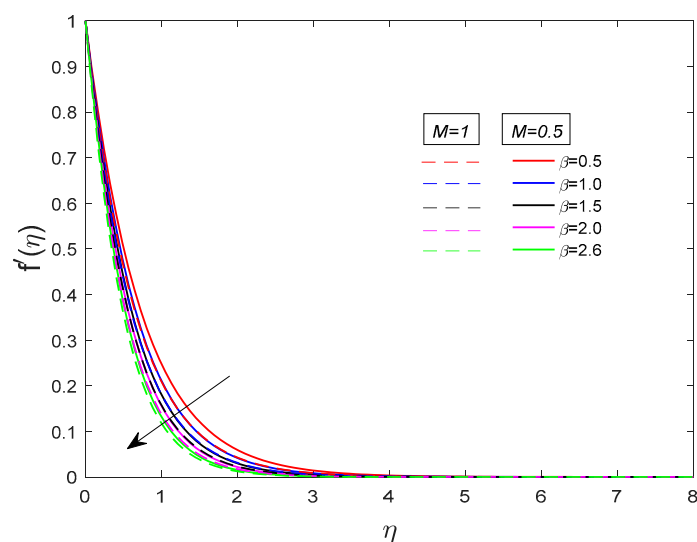


Figure 7. Effect of Maxwell fluid parameter (β) on axial velocity profile with $Pr = Sc = 0.7$, $Ec = Kr = Sr = 0.1$.

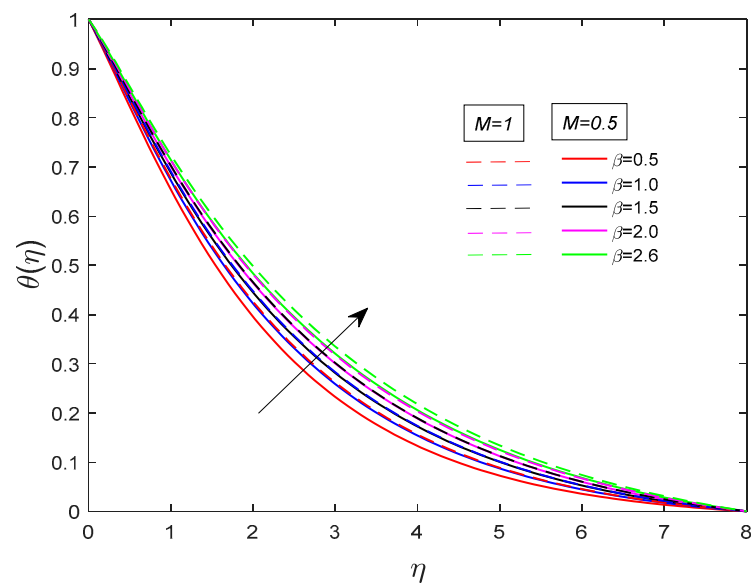


Figure 8. Effect of Maxwell fluid parameter (β) on temperature profile with $Pr = Sc = 0.7$, $Ec = Kr = Sr = 0.1$.

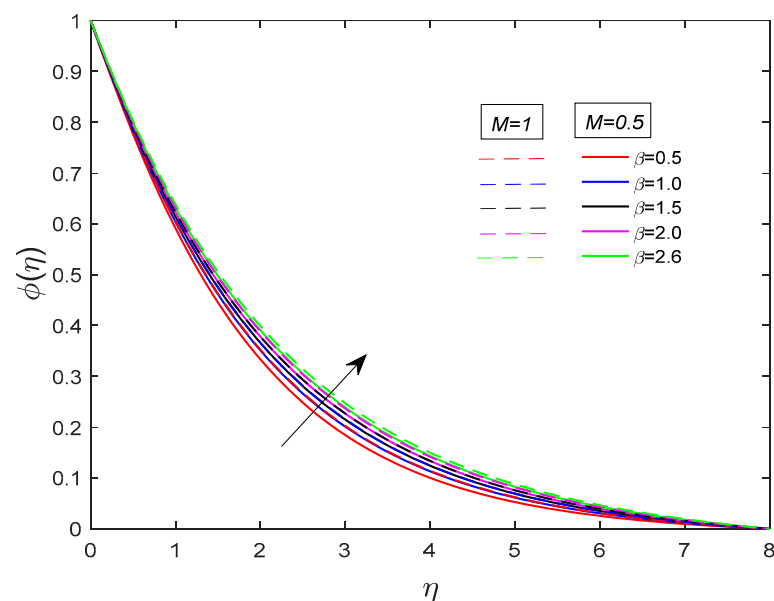


Figure 9. Impact of Maxwell fluid parameter (β) on concentration profile with $Pr = Sc = 0.7$, $Ec = Kr = Sr = 0.1$.

5.2.3. Effect of the Eckert Number (Ec)

Figures 10 and 11 describe the influence of Ec on temperature and concentration distribution profiles. It is recorded from Figure 10 that the enhancing Ec magnifies the thermal profile. The occurrence of frictional forces in the fluid medium acts as the source for the production of temperature energy in the liquid, and this situation strengthened the heat energy in the flow regime. This fact is well predicted in view of the Eckert number. Further, the Eckert number influences the heat energy because Ec directly influences the energy equation (refer to Equation (13)). Additionally, thickening the thermal boundary layer is considered for enhancing Ec values. Further, it is found from Figure 11 that enhancing the Eckert number decays the concentration distribution in the flow direction.

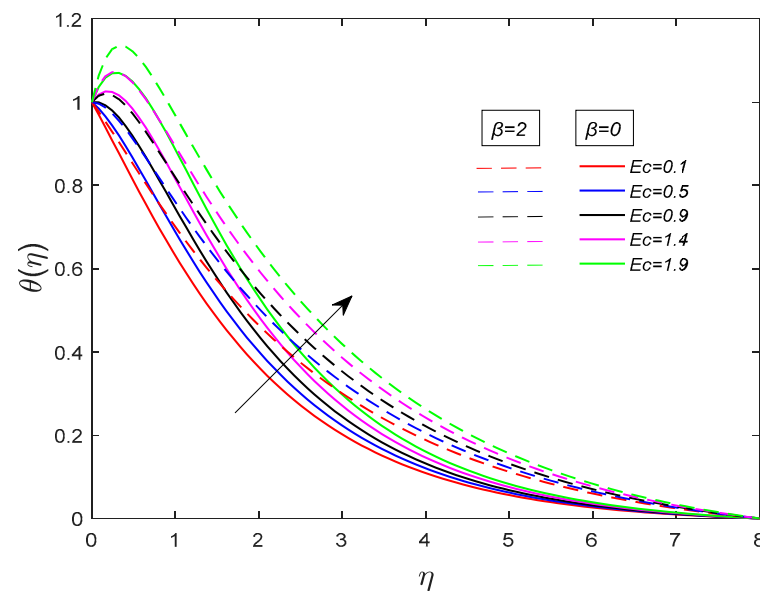


Figure 10. Influence of the Eckert number (Ec) on thermal profile with $Pr = 0.7$, $M = Kr = Sc = 0.5$, $Sr = 1.5$.

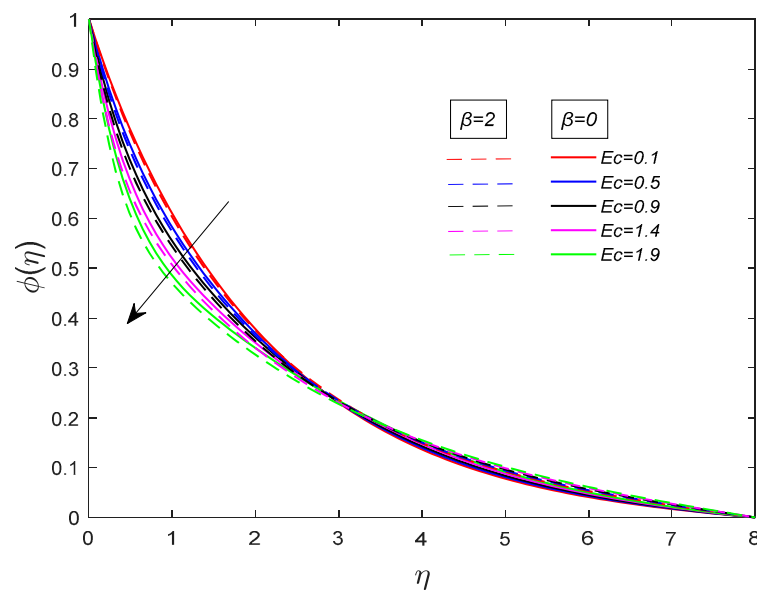


Figure 11. Effect of the Eckert number (Ec) on concentration profile with $Pr = 0.7$, $M = Kr = Sc = 0.5$, $Sr = 1.5$.

5.2.4. Impact of the Prandtl Number (Pr)

Figures 12 and 13 portray the influence of Pr on thermal and concentration fields for $\beta = 0$ and $\beta = 2$. Figure 12 demonstrates that the thermal profile decayed for rising Pr . Additionally, enhancing Pr diminished the temperature boundary layer thickness. Since the thermal diffusion of the fluid decays with the upsurge in Pr , and hence, thermal field decreases. Further, Figure 13 shows that the magnifying Pr enhances the concentration distribution in the flow regime.

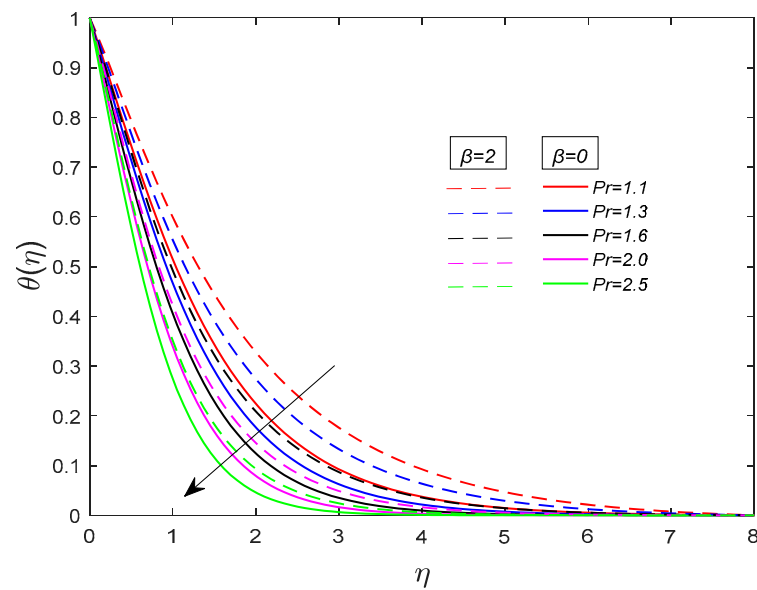


Figure 12. Effect of the Prandtl number (Pr) on thermal profile with $Ec = M = Kr = Sc = 0.5$, $Sr = 1.5$.

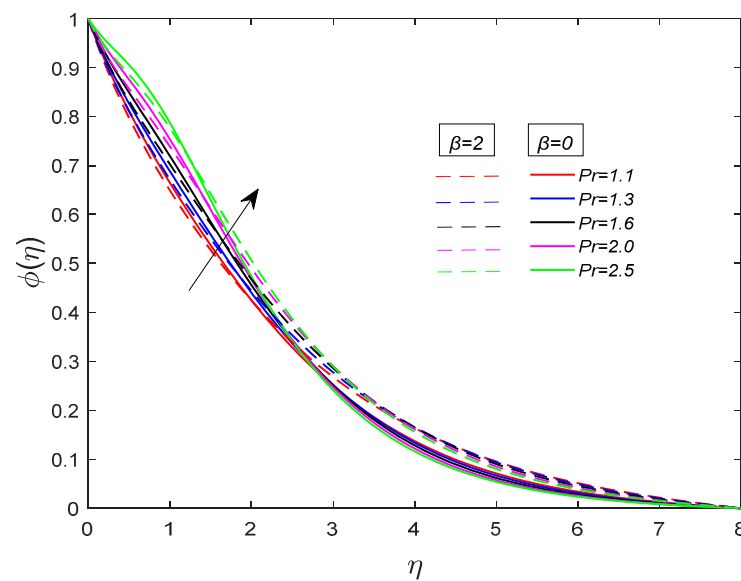


Figure 13. Effect of the Prandtl number (Pr) on concentration profiles with $Ec = M = Kr = Sc = 0.5$, $Sr = 1.5$.

5.2.5. Impact of the Schmidt Number (Sc) on Concentration Distribution

Figure 14 demonstrates the impact of Sc on concentration distribution for $\beta = 0$ and $\beta = 2$. It is clearly recorded from Figure 14 that the amplifying Sc decayed the concentration distribution in the boundary layer regime for $\beta = 0$ and $\beta = 2$. Concentration profile is a diminishing function of Sc because the greater Sc values are related to the lower mass diffusion, and hence, the concentration profile decreases. Additionally, the concentration boundary layer thickness is decayed with rising Sc .

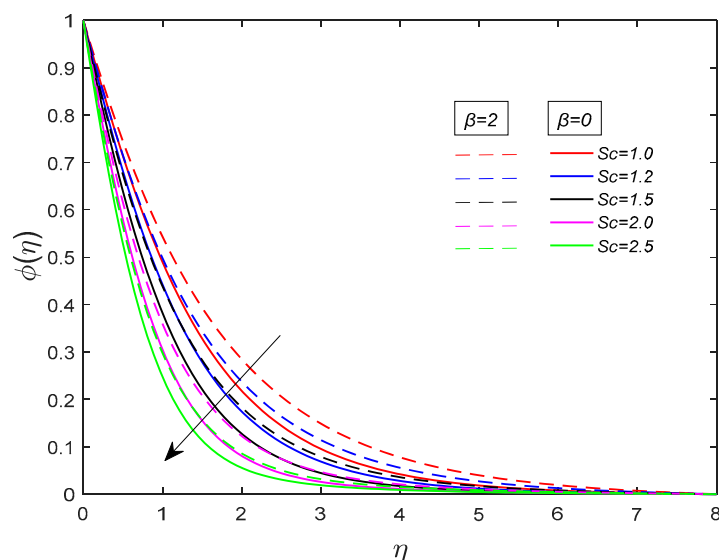


Figure 14. Effect of the Schmidt number (Sc) on concentration profile with $Pr = 0.7$, $M = 0.5$, $Ec = Kr = Sr = 0.1$.

5.2.6. Influence of the Soret Number (Sr)

Figure 15 illustrates the concentration distribution for various values of Sr for $\beta = 0$ and $\beta = 2$. The concentration distribution field is amplified for the enhancing values of Sr . This situation is due to the generation of extra mass fluxes due to the thermal gradients for the enhancing values of Sr . Additionally, the enhancing values of Sr magnifies the thermal boundary layer thickness.

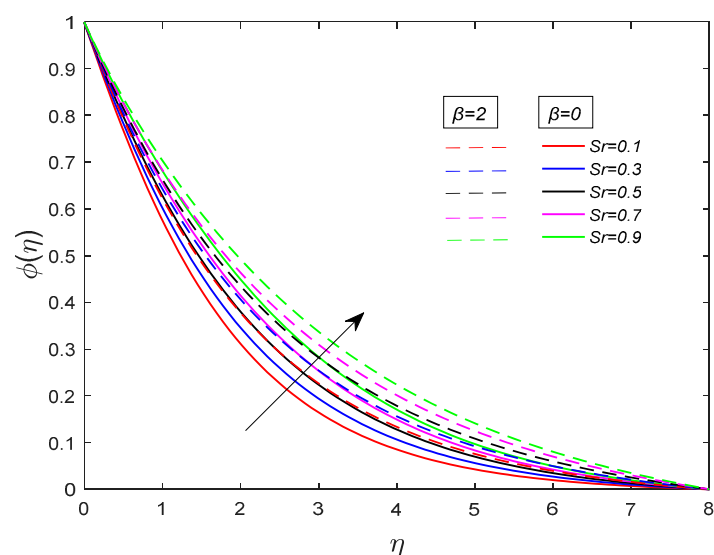


Figure 15. Effect of Soret parameter (Sr) on concentration profile with $Pr = Sc = 0.7$, $M = 0.5$, $Ec = Kr = 0.1$.

5.2.7. Influence of Chemical Reaction Parameter (Kr)

Influence of $\beta = 0$ and $\beta = 2$ for various values of Kr for both $Kr < 0$ (generative chemical reaction) and $Kr > 0$ (destructive chemical reaction) is demonstrated in Figure 16. Figure 16 reveals that the concentration distribution diminished for the magnifying Kr values. Additionally, the concentration distribution is greater for $\beta = 2$, when compared to $\beta = 0$ condition.

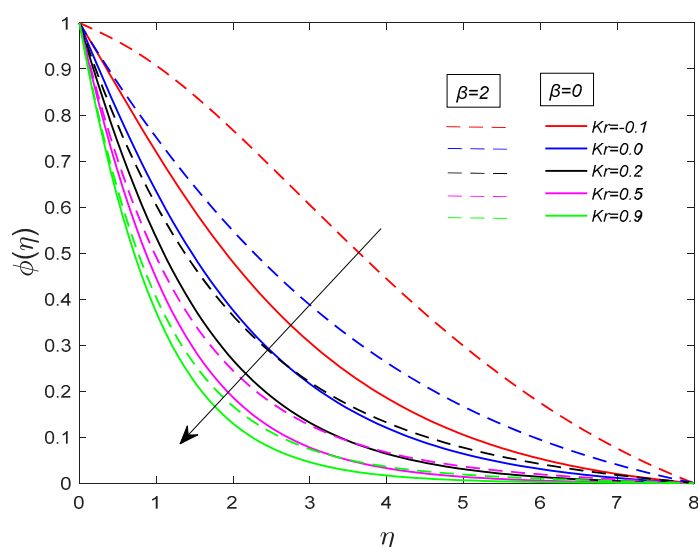


Figure 16. Effect of chemical reaction parameter (K_r) on concentration profile with $Pr = Sc = 0.7$, $M = 0.5$, $Ec = Sr = 0.1$.

5.3. Effect of Control Variables on Engineering Quantities

The impact of different physical parameters on momentum transport coefficient and heat and mass transport rates are illustrated in Table 2. It is clearly remarked from Table 2 that the rising magnetic parameter raises the value of the skin-friction coefficient and diminishes Nusselt and Sherwood numbers. Additionally, enhancing Maxwell fluid parameter magnifies the skin-friction coefficient and decays the thermal and concentration transport rates. Amplifying the Soret number decays the concentration transfer rate, and enhancing the chemical reaction parameter amplifies the Sherwood number.

Table 2. Impact of physical parameters on engineering quantities of interest.

M	β	Ec	Pr	Sr	Sc	Kr	$Cf_x Re_x^{0.5}$	$-Nu_x Re_x^{-0.5}$	$-Sh_x Re_x^{-0.5}$
0.1	0.5	0.1	0.7	0.1	0.7	0.1	1.16916	0.37399	0.48972
0.3							1.25083	0.35436	0.48166
0.5							1.32770	0.33654	0.47450
0.7							1.40050	0.32025	0.46809
0.5	1.0	0.1	0.7	0.1	0.7	0.1	1.42514	0.31172	0.46062
	1.5						1.51744	0.29046	0.44912
	2.0						1.60514	0.27206	0.43946
	2.5						1.68877	0.25595	0.43124
0.5	0.5	0.2	0.7	0.1	0.7	0.1	1.32770	0.28107	0.47810
		0.4					1.32770	0.17014	0.48530
		0.6					1.32770	0.05920	0.49250
		0.8					1.32770	−0.05172	0.49969
0.5	0.5	0.1	1.0	0.1	0.7	0.1	1.32770	0.43110	0.46910
			1.5				1.32770	0.56916	0.46115
			2.0				1.32770	0.68598	0.45431
			2.5				1.32770	0.78747	0.44826
0.5	0.5	0.1	0.7	0.2	0.7	0.1	1.32770	0.33654	0.46190
				0.4			1.32770	0.33654	0.43670
				0.6			1.32770	0.33654	0.41149
				0.8			1.32770	0.33654	0.38629
0.5	0.5	0.1	0.7	0.1	1.0	0.1	1.32770	0.33654	0.59678
					1.5		1.32770	0.33654	0.77300
					2.0		1.32770	0.33654	0.92528
					2.05		1.32770	0.33654	1.06103
0.5	0.5	0.1	0.7	0.1	0.7	−0.2	1.32770	0.33654	−0.04080
						−0.1	1.32770	0.33654	0.23554
						0.0	1.32770	0.33654	0.37598
						0.1	1.32770	0.33654	0.47450
						0.2	1.32770	0.33654	0.55321

6. Conclusions

The present numerical analysis deals with the study of heat and mass transfer behavior of the viscous incompressible time-independent laminar two-dimensional flow of Maxwell fluid over a stretching sheet under the influence of the Soret effect and magnetic field. In the present analysis, the behavior of non-Newtonian Maxwell fluid is differentiated from those of Newtonian fluids by using the well-known Maxwell fluid model. Further, the equations governing the 2D flow of viscous Maxwell fluid along the stretching sheet are derived and which are nonlinear and coupled in nature. Governing nonlinear system of partial differential equations are solved by utilizing the bvp4c MATLAB function. Additionally, numerical simulations are performed for various values of physical parameters. Further, the significant results of the present study are listed below.

- Normal and axial velocity fields decrease with the increasing values of M ;
- Temperature and concentration fields enhance with the rising values of M ;
- Normal and axial velocities decay with the rising values of β ;
- Thermal and concentration profiles increase with the rising values of β ;
- Enhancing the Soret parameter magnifies the concentration field in flow regime;
- Thermal profile decays with the enhancing values of Pr ;
- Concentration profile decreases with the enhancing values of Sc ;
- The magnitude of the skin-friction coefficient increases with rising values of M and β ;
- The Nusselt number increases with increasing values of Pr ;
- The Sherwood number magnifies with enhancing values of Sc and Kr .

Author Contributions: Conceptualization, H.B. and G.J.R.; methodology, S.S.P., H.B. and G.J.R.; software, H.B.; writing—original draft preparation, S.S.P., H.B., G.J.R. and M.A.S.; writing—review and editing, S.S.P., H.B., G.J.R. and M.A.S.; visualization, S.S.P. and H.B. All authors have read and agreed to the published version of the manuscript.

Funding: This research received no external funding.

Institutional Review Board Statement: Not applicable.

Informed Consent Statement: Not applicable.

Data Availability Statement: Not applicable.

Acknowledgments: The first author wishes to thank Government of India, Ministry of Human Resource Development (MHRD), University Grant Commission (UGC), for the grant of research fellowship ((Reg. No: 400170), (UGC Ref. No: 956/(CSIR-NET JUNE-2018)) and to the Central university of Karnataka for providing the research facilities and this research of Mikhail A. Sheremet was supported by the TPU development program.

Conflicts of Interest: The authors declare no conflict of interest.

Nomenclature

C	Concentration distribution
f', f	Non-dimensional flow components
k	Thermal conductivity of the fluid
Kr	Chemically reaction parameter
M	Magnetic parameter
Pr	Prandtl number
Sc	Schmidt number
Sr	Soret number
T	Temperature distribution
u, v	Flow components along x, y directions
Greek symbols	
α	Thermal diffusivity
β	Maxwell fluid parameter
η	Similarity variable
θ	Dimensionless temperature

φ	Dimensionless concentration
ψ	Stream function
μ	Dynamic viscosity
ν	Kinematic viscosity
ρ	Fluid density
Subscripts	
w	Surface conditions
∞	Ambient conditions

References

- Schulz, D.N.; Glass, J.E. *Polymers as Rheology Modifiers*; ACS Symposium Series 462; American Chemical Society: Washington, DC, USA, 1991.
- Sakiadis, B.C. Boundary-layer behaviour on continuous solid surfaces: I. Boundary-layer equations for two-dimensional and axisymmetric flow. *Am. Inst. Chem. Eng. J.* **1961**, *7*, 26–28. [\[CrossRef\]](#)
- Sakiadis, B.C. Boundary-layer behaviour on continuous solid surfaces: II. Boundary-layer on a continuous flat surface. *Am. Inst. Chem. Eng. J.* **1961**, *7*, 221–225. [\[CrossRef\]](#)
- Phan-Thien, N. Plane and axi-symmetric stagnation flow of a Maxwellian fluid. *Rheol. Acta* **1983**, *22*, 127–130. [\[CrossRef\]](#)
- Zheng, R.; Phan-Thien, N.; Tanner, R.I. On the flow past a sphere in a cylindrical tube: Limiting Weissenberg number. *J. Non-Newton. Fluid Mech.* **1990**, *36*, 27–49. [\[CrossRef\]](#)
- Sadeghy, K.; Najaf, A.-H.; Saffaripour, M. Sakiadis flow of an upper-convected Maxwell fluid. *Int. J. Non-Linear Mech.* **2005**, *40*, 1220–1228. [\[CrossRef\]](#)
- Hayat, T.; Abbas, Z.; Sajid, M. Series solution for the upper-convected Maxwell fluid over a porous stretching plate. *Phys. Lett. A* **2006**, *358*, 396–403. [\[CrossRef\]](#)
- Hayat, T.; Sajid, M. Homotopy analysis of MHD boundary layer flow of an upper-convected Maxwell fluid. *Int. J. Eng. Sci.* **2007**, *45*, 393–401. [\[CrossRef\]](#)
- Abbas, Z.; Hayat, T.; Sajid, M.; Asghar, S. Unsteady flow of a second grade fluid film over an unsteady stretching sheet. *Math. Comput. Model.* **2008**, *48*, 518–526. [\[CrossRef\]](#)
- Abbas, Z.; Wang, Y.; Hayat, T.; Oberlack, M. Mixed convection in the stagnation point flow of a Maxwell fluid towards a vertical stretching surface. *Nonlinear Anal. Real World Appl.* **2010**, *11*, 3218–3228. [\[CrossRef\]](#)
- Hayat, T.; Awais, M.; Qasim, M.; Hendi, A.A. Effects of mass transfer on the stagnation point flow of an upper-convected Maxwell (UCM) fluid. *Int. J. Heat Mass Transf.* **2011**, *54*, 3777–3782. [\[CrossRef\]](#)
- Ishak, A.; Nazar, R.; Arifin, N.M.; Pop, I. Dual solutions in mixed convection flow near stagnation point on a vertical porous plate. *Int. J. Therm. Sci.* **2008**, *47*, 417–422. [\[CrossRef\]](#)
- Sahoo, B. Effects of slip, viscous dissipation and Joule heating on the MHD flow and heat transfer of a second grade fluid past a radially stretching sheet. *Appl. Math. Mech.* **2010**, *31*, 159–173. [\[CrossRef\]](#)
- Ijaz, M.; Ayub, M. Thermally stratified flow of Jeffrey fluid with homogeneous-heterogeneous reactions and non-Fourier heat flux model. *Heliyon* **2019**, *5*, e02303. [\[CrossRef\]](#) [\[PubMed\]](#)
- Sandeep, N.; Sulochana, C. Momentum and heat transfer behaviour of Jeffrey, Maxwell and Oldroyd-B nanofluids past a stretching surface with non-uniform heat source/sink. *Ain Shams Eng. J.* **2018**, *9*, 517–524. [\[CrossRef\]](#)
- Ramzan, M.; Bilal, M.; Chung, J.D. Effects of thermal and solutal stratification on Jeffrey magneto-nanofluid along an inclined stretching cylinder with thermal radiation and heat generation/absorption. *Int. J. Mech. Sci.* **2017**, *131*, 317–324. [\[CrossRef\]](#)
- Khan, M.I.; Waqas, M.; Hayat, T.; Alsaedi, A. Soret and Dufour effects in stretching flow of Jeffrey fluid subject to Newtonian heat and mass conditions. *Results Phys.* **2017**, *7*, 4183–4188. [\[CrossRef\]](#)
- Hayat, T.; Qayyum, S.; Farooq, M.; Alsaedi, A.; Ayub, M. Mixed convection flow of Jeffrey fluid along an inclined stretching cylinder with double stratification effect. *Therm. Sci.* **2017**, *21*, 849–862. [\[CrossRef\]](#)
- Zeeshan, A.; Majeed, A. Heat transfer analysis of Jeffrey fluid flow over a stretching sheet with suction/injection and magnetic dipole effect. *Alex. Eng. J.* **2016**, *55*, 2171–2181. [\[CrossRef\]](#)
- Hayat, T.; Qayyum, S.; Imtiaz, M.; Alsaedi, A. Three-dimensional rotating flow of Jeffrey fluid for Cattaneo-Christov heat flux model. *Aip Adv.* **2016**, *6*, 025012. [\[CrossRef\]](#)
- Abbasi, F.M.; Shehzad, S.A.; Hayat, T.; Alsaedi, A.; Obid, M.A. Influence of heat and mass flux conditions in hydromagnetic flow of Jeffrey nanofluid. *Aip. Adv.* **2015**, *5*, 037111. [\[CrossRef\]](#)
- Hayat, T.; Asad, S.; Alsaedi, A.; Alsaadi, F.E. Radiative flow of Jeffrey fluid through a convectively heated stretching cylinder. *J. Mech.* **2015**, *31*, 69–78. [\[CrossRef\]](#)
- Farooq, M.; Gull, N.; Alsaedi, A.; Hayat, T. MHD flow of a Jeffrey fluid with Newtonian heating. *J. Mech.* **2015**, *31*, 319–329. [\[CrossRef\]](#)
- Hayat, T.; Asad, S.; Alsaedi, A. Analysis for flow of Jeffrey fluid with nanoparticles. *Chin. Phys. B* **2015**, *24*, 044702. [\[CrossRef\]](#)
- Liu, Y.Q.; Guo, B.L. Coupling model for unsteady MHD flow of generalized Maxwell fluid with radiation thermal transfer. *Appl. Math. Mech.* **2016**, *37*, 137–150. [\[CrossRef\]](#)

26. Li, C.R.; Zheng, L.C.; Zheng, X.X.; Chen, G. Flow and heat transfer of a generalized Maxwell fluid with modified fractional Fourier's law and Darcy's law. *Comput. Fluids* **2016**, *125*, 25–38. [\[CrossRef\]](#)
27. Zhang, Y.; Zheng, L.C.; Wang, X.J.; Song, G.H. Analysis of Marangoni convection of non-Newtonian power law fluids with linear temperature distribution. *Therm. Sci.* **2011**, *15*, 45–52. [\[CrossRef\]](#)
28. Zhang, C.L.; Zheng, L.C.; Zhang, X.X.; Chen, G. MHD flow and radiation heat transfer of nanofluids in porous media with variable surface heat flux and chemical reaction. *Math. Comput. Model.* **2015**, *39*, 165–181. [\[CrossRef\]](#)
29. Shen, B.Y.; Zheng, L.C.; Chen, S.T. Fractional boundary layer flow and radiation heat transfer of MHD viscoelastic fluid over an unsteady stretching surface. *AIP Adv.* **2015**, *5*, 107133–107134. [\[CrossRef\]](#)
30. Rachid, H. Effects of heat transfer and an endoscope on peristaltic flow of a fractional Maxwell fluid in a vertical tube. *Abstr. Appl. Anal.* **2015**, *1*, 1–9. [\[CrossRef\]](#)
31. Waheed, S.E. Flow and heat transfer in a Maxwell liquid film over an unsteady stretching sheet in a porous medium with radiation. *SpringerPlus* **2016**, *5*, 1–14. [\[CrossRef\]](#)
32. Guinness, I.G. Theorie Analytique De La Chaleur (1822). *Land Mark Writ. West. Math.* **2005**, *1640–1940*, 354–365. [\[CrossRef\]](#)
33. Cattaneo, C. Sulla conduzionedelcalore. *Atti Semin. Mat. Fis. Univ. Modena* **1948**, *3*, 83–101.
34. Christov, C.I. On frame indifferent formulation of the Maxwell–Cattaneo model of finite-speed heat conduction. *Mech. Res. Commun.* **2009**, *36*, 481–486. [\[CrossRef\]](#)
35. Tibullo, V.; Zampoli, V. A uniqueness result for the Cattaneo–Christov heat conduction model applied to incompressible fluids. *Mech. Res. Commun.* **2011**, *38*, 77–79. [\[CrossRef\]](#)
36. Han, S.; Zheng, L.; Li, C.; Zhang, X. Coupled flow and heat transfer in viscoelastic fluid with Cattaneo–Christov heat flux model. *Appl. Math. Lett.* **2014**, *38*, 87–93. [\[CrossRef\]](#)
37. Zheng, L.C.; Liu, N.; Zhang, X.X. Maxwell fluids unsteady mixed flow and radiation heat transfer over a stretching permeable plate with boundary slip and non-uniform heat source/sink. *J. Heat Transf.* **2013**, *135*, 1–6. [\[CrossRef\]](#)
38. Siddiqui, A.M.; Rana, M.A.; Ahmed, N. Effects of hall current and heat transfer on MHD flow of a Burgers' fluid due to a pull of eccentric rotating disks. *Commun. Nonlinear Sci. Numer. Simul.* **2008**, *13*, 1554–1570. [\[CrossRef\]](#)
39. Ezzat, M.A.; El-Bary, A.A. Effects of variable thermal conductivity on Stokes' flow of a thermoelectric fluid with fractional order of heat transfer. *Int. J. Therm. Sci.* **2016**, *100*, 305–315. [\[CrossRef\]](#)
40. Hayat, T.; Ashraf, M.B.; Alsaedi, A.; Alhothuali, M.S. Soret and Dufour effects in three-dimensional flow of Maxwell fluid with chemical reaction and convective condition. *Int. J. Numer. Methods Heat Fluid Flow* **2015**, *25*, 98–120. [\[CrossRef\]](#)
41. Srinivasulu, T.; Goud, B.S. Effect of inclined magnetic field on flow, heat and mass transfer of Williamson nanofluid over a stretching sheet. *Case Stud. Therm. Eng.* **2021**, *23*, 100819. [\[CrossRef\]](#)
42. Khana, N.A.; Sultan, F. MHD flow of a Williamson fluid over an infinite rotating disk with anisotropic slip. *J. Eng. Phys. Thermophys.* **2019**, *92*, 1625–1636. [\[CrossRef\]](#)
43. Shafiq, A.; Rashidib, M.M.; Hammouchand, Z.; Khan, I. Analytical investigation of stagnation point flow of Williamson liquid with melting phenomenon. *Phys. Scr.* **2018**, *94*, 035204. [\[CrossRef\]](#)
44. Rasool, G.; Zhang, T.; Chamkha, A.J.; Shafiq, A.; Tlili, I.; Shahzadi, G. Entropy generation and consequences of binary chemical reaction on MHD Darcy–Forchheimer Williamson nanofluid flow over non-linearly stretching surface. *Entropy* **2020**, *22*, 18. [\[CrossRef\]](#) [\[PubMed\]](#)
45. Hamid, A.; Khan, M.; Alghamdi, M. Numerical simulation for transient flow of Williamson fluid with multiple slip model in the presence of chemically reacting species. *Int. J. Numer. Methods Heat Fluid Flow* **2019**, *29*, 4445–4461. [\[CrossRef\]](#)
46. Hamid, A.; Khan, M. Multiple solutions for MHD transient flow of Williamson nanofluids with convective heat transport. *J. Taiwan Inst. Chem. Eng.* **2019**, *103*, 126–137.
47. Khan, M.I.; Qayyum, S.; Hayat, T.; Khan, M.I.; Alsaedi, A. Entropy optimization in flow of Williamson nanofluid in the presence of chemical reaction and Joule heating. *Int. J. Heat Mass Transf.* **2019**, *133*, 959–967. [\[CrossRef\]](#)
48. Khan, M.; Salahuddin, T.; Yousaf, M.M.; Khan, F.; Hussain, A. Variable diffusion and conductivity change in 3D rotating Williamson fluid flow along with magnetic field and activation energy. *Int. J. Numer. Methods Heat Fluid Flow* **2020**, *30*, 2467–2484. [\[CrossRef\]](#)
49. Kendoush, A.A. Theory of stagnation region heat and mass transfer to fluid jets impinging normally on solid surfaces. *Chem. Eng. Process. Process. Intensif.* **1998**, *37*, 223–228. [\[CrossRef\]](#)
50. Liu, I.C. A note on heat and mass transfer for a hydromagnetic flow over a stretching sheet. *Int. Commun. Heat Mass Transf.* **2005**, *32*, 1075–1084. [\[CrossRef\]](#)
51. Cortell, R. Toward an understanding of the motion and mass transfer with chemically reactive species for two classes of viscoelastic fluid over a porous stretching sheet. *Chem. Eng. Process. Process. Intensif.* **2007**, *46*, 982–989. [\[CrossRef\]](#)
52. Andersson, H.I.; Hansen, O.R.; Holmedal, B. Diffusion of a chemically reactive species from a stretching sheet. *Int. J. Heat Mass Transf.* **1994**, *37*, 659–664. [\[CrossRef\]](#)
53. Takhar, H.S.; Chamkha, A.J.; Nath, G. Flow and mass transfer on a stretching sheet with magnetic field and chemical reactive species. *Int. J. Eng. Sci.* **2000**, *38*, 1303–1314. [\[CrossRef\]](#)
54. Akyildiz, F.T.; Bellout, H.; Vajravelu, K. Diffusion of chemical reactive species in porous medium over a stretching sheet. *J. Math. Anal. Appl.* **2006**, *320*, 322–339. [\[CrossRef\]](#)

55. Layek, G.C.; Mukhopadhyay, S.; Samad, S.A. Heat and mass transfer analysis for boundary layer stagnation-point flow towards a heated porous stretching sheet with heat absorption/generation and suction/blowing. *Int. Commun. Heat Mass Transf.* **2007**, *34*, 347–356. [[CrossRef](#)]
56. Hayat, T.; Awais, M.; Sajid, M. Similar solutions of stretching flow with mass transfer. *Int. J. Numer. Methods Fluids* **2009**, *64*, 908–921. [[CrossRef](#)]
57. Hayat, T.; Awais, M. Simultaneous effects of heat and mass transfer on time-dependent flow over a stretching surface. *Int. J. Numer. Methods Fluids* **2011**, *67*, 1341–1357. [[CrossRef](#)]
58. Raza, J.; Oudina, F.M.; Mahanthesh, B. Magnetohydrodynamic flow of nano Williamson fluid generated by stretching plate with multiple slips. *Multidiscip. Modeling Mater. Struct.* **2019**, *15*, 871–894. [[CrossRef](#)]
59. Shawky, H.M.; Eldabe, N.T.M.; Kamel, K.A.; Abd-Aziz, E.A. MHD flow with heat and mass transfer of Williamson nanofluid over stretching sheet through porous medium. *Microsyst. Technol.* **2019**, *25*, 1155–1169. [[CrossRef](#)]
60. Loganathan, K.; Rajan, S. An entropy approach of Williamson nanofluid flow with Joule heating and zero nanoparticle mass flux. *J. Therm. Anal. Calorim.* **2020**, *141*, 2599–2612. [[CrossRef](#)]
61. Salahuddin, T. Modelling unsteady waveform Williamson fluid flow near a permeable radioactive surface. *Int. Commun. Heat Mass Transf.* **2020**, *117*, 104764. [[CrossRef](#)]
62. Dada, M.S.; Onwubuoya, C. Variable viscosity and thermal conductivity effects on Williamson fluid flow over a slendering stretching sheet. *World J. Eng.* **2020**, *17*, 357–371. [[CrossRef](#)]
63. Kumar, A.; Tripathi, R.; Singh, R.; Chaurasiya, V.K. Simultaneous effects of nonlinear thermal radiation and Joule heating on the flow of Williamson nanofluid with entropy generation. *Phys. A* **2020**, *551*, 123972. [[CrossRef](#)]
64. Khan, M.I.; Javed, S.; Hayat, T.; Waqas, M.; Alsaedi, A. Entropy optimization in cubic autocatalysis chemical reactive flow of Williamson fluid subjected to viscous dissipation and uniform magnetic field. *J. Cent. South Univ.* **2019**, *26*, 1218–1232. [[CrossRef](#)]
65. Abel, M.S.; Tawade, J.V.; Nandeppanavar, M.M. MHD flow and heat transfer for the upper-convected Maxwell fluid over a stretching sheet. *Meccanica* **2012**, *47*, 385–393.
66. Sadeghy, K.; Hajibeygi, H.; Taghavi, S.M. Stagnation point flow of upper-convected Maxwell fluids. *Int. J. Non-Linear Mech.* **2006**, *41*, 1242–1247. [[CrossRef](#)]
67. Basha, H.; Reddy, G.J.; Abhishek Annapoorna, K.; Vianaya, P.; Kumar, N.N. Numerical modelling of second-grade fluid flow past a stretching sheet. *Heat Transf. Asian Res.* **2019**, *48*, 1595–1621. [[CrossRef](#)]